

## The Momentum Distribution of Projectile Fragments

Fragments with beam-like velocities are observed at forward scattering angles in heavy-ion reactions at all bombarding energies above the Coulomb barrier. The spread in momentum of these fragments,  $\sigma$ , and particularly the variation of  $\sigma$  with bombarding energy, are of current interest. The present experimental data and their theoretical interpretations are summarized. New detector systems are now beginning to deliver results that promise to increase our understanding of the transition region in which  $\sigma$  increases with energy (10–100 MeV/n) and the high energy limit where the widths appear constant (above 200 MeV/n).

### INTRODUCTION

If a moving balloon filled with water grazes the point of a knife we would expect a shower of water droplets moving with the same average velocity as the balloon. Furthermore, the number, sizes, and individual velocities of the droplets should tell us something about the state of the balloon and its contents before it encountered the knife.

Although the differences between a heavy-ion projectile and a water-filled balloon are legion, the analogy does help explain the persistence in heavy-ion reaction spectra of the quasi-elastic peak—a characteristic group of fragments having masses less than the projectile mass and a distribution of velocities whose average is close to that of the beam velocity. This is illustrated schematically in Figure 1. Projectile  $P$  collides with target nucleus  $T$  and produces a fragment

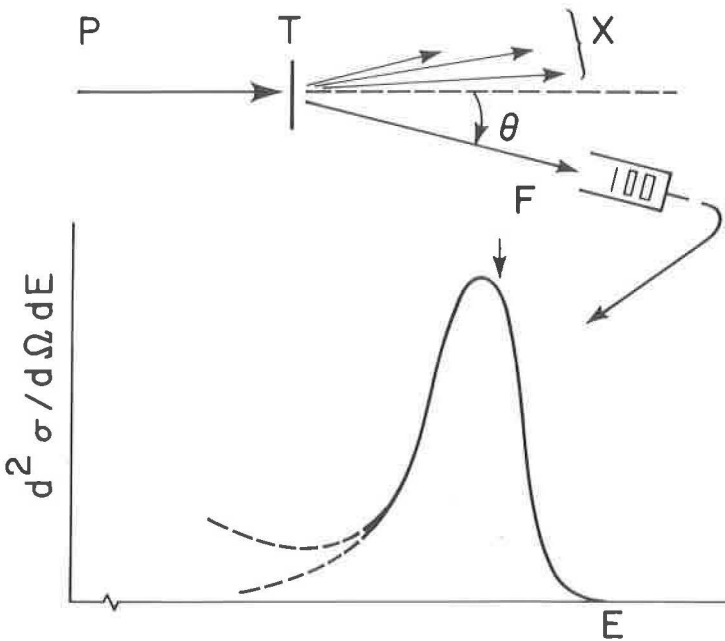


FIGURE 1 Schematic illustration of an inclusive reaction in which projectile  $P$  collides with target nucleus  $T$  to produce one or more fragments at forward angles. All unobserved particles are denoted by  $X$ . A typical energy spectrum for the detected particle  $F$  is indicated. The arrow denotes the energy corresponding to the beam velocity. Depending on the particular reaction, the shape of the peak may vary on the low energy side.

$F$  at an angle  $\theta$  near the classical grazing angle. The unobserved products of the reaction are denoted by  $X$ . This type of inclusive measurement has been performed at bombarding energies ranging from the Coulomb barrier upward to 2000 MeV/n. As indicated in Figure 1, there is a small downward shift of the peak of the distribution relative to the beam velocity. This is expected because some initial kinetic energy is converted to internal excitation. What is of more interest here is the momentum width,  $\sigma$ , of the fragment distribution. These widths, experiments show, depend on the masses of the projectile and the fragment and hardly at all on the mass of the

target.<sup>1,2</sup> There is, however, a pronounced dependence on the bombarding energy:  $\sigma$  appears to reach asymptotic values at low and high bombarding energies, and to exhibit a relatively rapid transition from one limit to the other. In this Comment I will give a brief description of the experimental and theoretical work underlying our present understanding of momentum widths and then discuss new experiments that may substantially increase this understanding.

## EXPERIMENTAL RESULTS AT HIGH ENERGIES: THE DEVELOPMENT OF THE STATISTICAL MODEL

In the early 1970s, a series of experiments<sup>1</sup> was made using relativistic <sup>12</sup>C and <sup>16</sup>O projectiles and a variety of targets from Be to Pb. For a given fragment the distribution of momenta in the direction parallel to the beam was found to be a Gaussian in the rest frame of the projectile (Figure 2). The variance of this distribution,  $\sigma^2$ , had a parabolic dependence on fragment mass (Figure 3). These pioneering experiments inspired theoretical interpretations<sup>3,4</sup> that remain the starting point for more sophisticated models. The basic idea is that the interaction with the target effectively produces a fragment consisting of a number of nucleons chosen at random from the projectile. One mechanism for this has been described<sup>3</sup> as follows: "The target nucleus acts only to inject energy into the incident heavy ion, causing it to 'explode' into a number of fragments." In this picture the momentum of a fragment is given essentially by the momentum it had relative to the center of mass of the projectile just prior to the collision. If the distribution of momenta is known for the individual nucleons within the projectile, the momentum distribution can be calculated for a fragment consisting of nucleons chosen at random. Goldhaber<sup>4</sup> showed that

$$\sigma_{\parallel}^2 = \frac{\langle p^2 \rangle}{3} \frac{A_F(A_P - A_F)}{A_P - 1} \equiv \sigma_0^2 \frac{A_F(A_P - A_F)}{A_P - 1}, \quad (1)$$

where  $A_P$  and  $A_F$  denote the atomic weights of the projectile and fragment, respectively. For a Fermi gas, the mean square momentum of the individual nucleons is  $\langle p^2 \rangle = \frac{3}{5} p_f^2$  where  $p_f$  is the Fermi momentum.

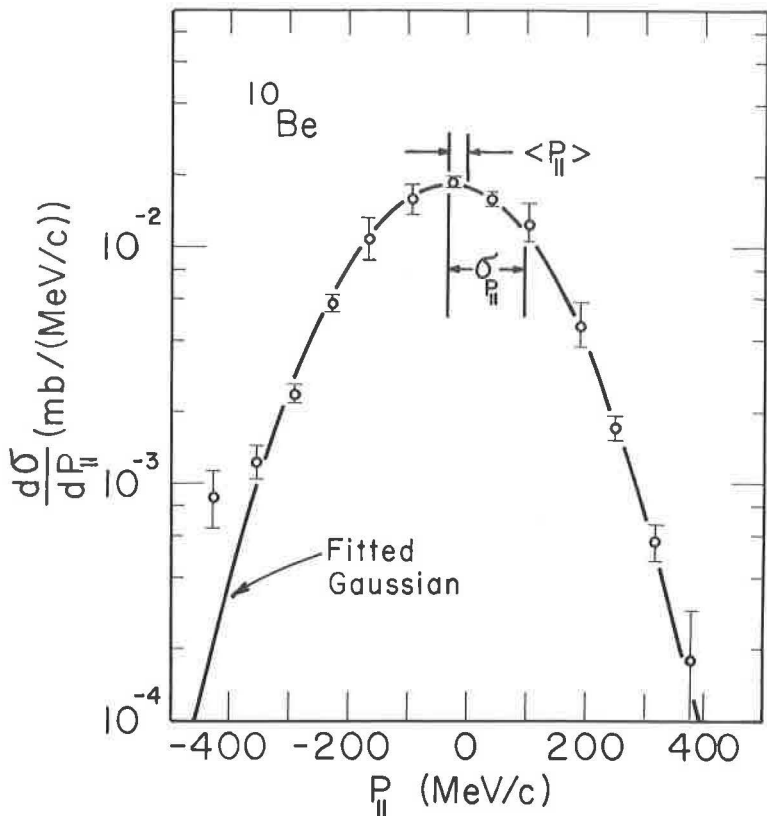


FIGURE 2 The momentum distribution in the rest frame of the projectile and parallel to the beam axis for  $^{10}\text{Be}$  fragments produced by a 2.1 GeV/n beam of  $^{12}\text{C}$  ions on a Be target.<sup>1</sup> The mean momentum  $\langle p_{||} \rangle$  and the standard deviation  $\sigma_{||}$  are -30 and 129  $\text{MeV}/c$ , respectively.

In view of its simplicity, this picture is remarkably successful (see Gelbke *et al.*),<sup>2</sup> with the fitted value of  $\sigma_0$  being about 10%–20% lower than the value of  $\sim 100 \text{ MeV}/c$  based on  $p_f$  as determined by electron scattering. The conclusion is that projectile fragmentation at relativistic energies is governed by the nuclear structure (i.e., the Fermi statistics) of the projectile alone.

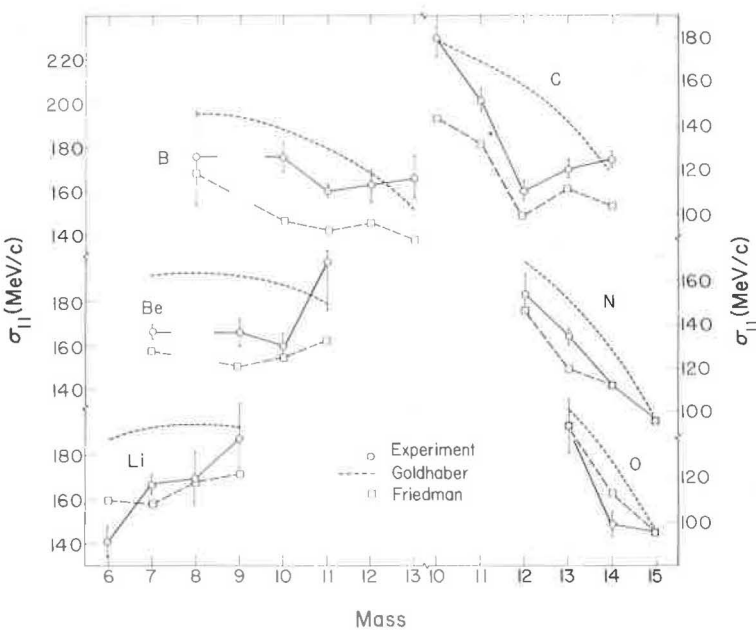


FIGURE 3 Experimental momentum widths, compared to the parabolic prediction of Goldhaber<sup>4</sup> and the predictions of the peripheral model of Friedman.<sup>6</sup>

#### THEORETICAL DEVELOPMENT OF THE STATISTICAL MODEL: ALTERNATIVE VIEWS

A number of significant modifications of the early statistical models have been made in recent years. The basic assumptions of the statistical model (that the nucleonic motion is uncorrelated and that the nucleons in the fragment are chosen at random) have been reexamined by Bertsch,<sup>5</sup> Friedman,<sup>6</sup> and Murphy.<sup>7</sup> Bertsch calculated the effect of the Pauli exclusion principle on the momenta of the nucleons that make up the fragment. Since the exclusion principle requires large anticorrelations in the momenta of identical fermions when they are close together in space, the quantity  $\langle \mathbf{p}_i \cdot \mathbf{p}_j \rangle$  takes on a more negative value than derived by Goldhaber. For the case of an  ${}^{40}\text{Ar}$  projectile that is sheared in half, the predicted momentum dispersion

$(\sigma^2)$  and the experimental value<sup>8</sup> are in much better agreement, each being, respectively, 37% and 31% less than the value predicted for no correlations.

Another constraint on the momenta of the projectile-like fragments has been considered by Murphy.<sup>7</sup> The nucleons in the projectile cannot be sampled completely at random because of the requirement that the fragment to be observed must be a nucleus, e.g., a Fermi gas. This limits the available configurations in the projectile, and, hence, reduces the predicted momentum widths.

The peripheral nature of fragmentation reactions—that a surviving fragment must not have interacted strongly with the target—is emphasized by Friedman.<sup>6</sup> In this picture the target removes nucleons only from the near side of projectile's surface and the relevant momentum is that of the cluster of nucleons in the tail of the wavefunction,  $\psi(r)$ :

$$\psi_{F-R}(r) \simeq e^{-\mu r} / r_s \quad (2)$$

(The projectile is considered as two pieces, the group of nucleons comprising the removed portion  $R$  and the remaining fragment  $F$  that is observed.) In Equation (2),  $\mu = \sqrt{2m_s E_s}$  where  $m_s$  is the reduced mass of the clusters  $F$  and  $R$ , and  $E_s$  is their separation energy. The momentum distribution thus depends directly on the separation energy of the particular fragment rather than on the Fermi energy. The variation of separation energies from one fragment nucleus to another introduces variations in  $\sigma$  that generally improve the agreement with experiment relative to the predictions of Eq. (1). This is illustrated in Figure 3.

The predictions of the surface cluster model of Friedman are similar to the simple statistical model, viz., they indicate an approximately parabolic mass dependence. The connection of the two models has been discussed by Friedman and turns on the close relationship of the separation energy (per nucleon) to the Fermi energy. In principle, any nuclear structure or correlation effects that go beyond conservation of momentum and a Fermi-gas picture, and any spatial restrictions on the selection of nucleons, will reduce the predicted value of  $\sigma_0$ . However, there has not been a unified theoretical treatment

that takes into account simultaneously the different factors that reduce  $\sigma_0^2$  below the value  $p_f^2/5$ .

The observation of a Gaussian momentum distribution, by itself, does not tell us very much about the specific reaction mechanism. Thus it should not be surprising that alternatives to the above models exist. Instead of an instantaneous snapshot of the projectile with the distribution of momenta governed by the interior of the cold projectile nucleus before the collision (as diagrammed in Figure 4a), one may suppose a postcollision equilibration<sup>4</sup> and that the distribution of momenta reflects the thermalized energy of excitation in the projectile acquired via the collision (Figure 4b). In this case the variance also has essentially the same form as Eq. (1) and  $\sigma_0$  is directly proportional to the temperature of the system.

Thus,

$$\sigma^2 = m_N k T \frac{A_F(A_P - A_F)}{A_P},$$

where  $m_N$  is the mass of the nucleon,  $k$  is Boltzmann's constant, and  $T$  is the temperature of the equilibrated system.<sup>4</sup> Temperatures of 7–9 MeV per nucleon are required to reproduce the data at relativistic energies. In this view the entire process is described<sup>9,10</sup> by two stages: (i) abrasion, the fast process in which the target deposits energy in and removes nucleons from the projectile, thereby producing an excited fragment, and (ii) ablation, a slower process in which the remaining fragment reaches equilibrium and evaporates neutrons, protons, alpha particles, etc. One may of course arrive at a distribution of momenta and isotopes without necessarily first removing nucleons in the abrasion stage. Such a process is just the excitation of the projectile by inelastic scattering to states above particle decay thresholds, followed by sequential emission. (This phenomenon is well known from experiments at low energies.) The variation in fragment momentum arises from the recoil imparted when nucleons or clusters are evaporated and, for lighter projectiles, this variation may depend sensitively on the thresholds for particle decay.

We are thus faced with a situation in which the present high energy inclusive data—the widths of momentum distributions and the isotope yields—are sufficient to establish a statistical process involving the projectile alone, but are insufficient to determine whether this is a fast or a slow mechanism.

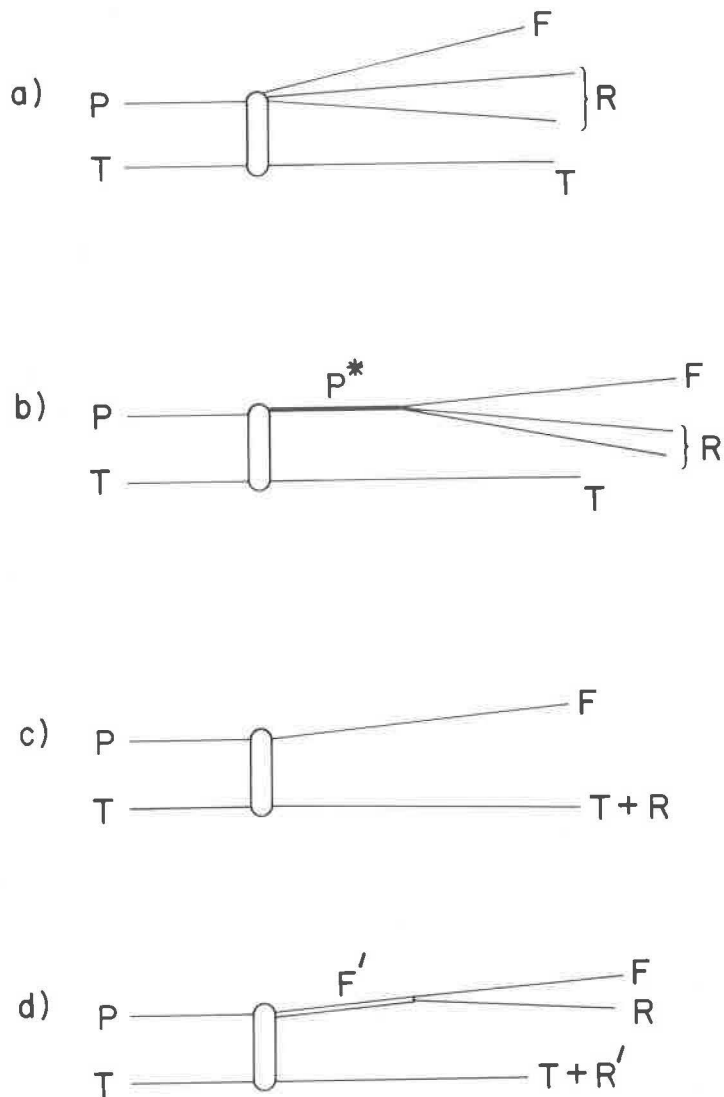


FIGURE 4 A schematic illustration of the different processes that may contribute to the formation of projectile-like fragments,  $F$ , unobserved fragments,  $R$ , and target-like residues. (a) Prompt fragmentation; (b) equilibration of an excited projectile  $P^*$ , followed subsequently by particle decay; (c) a transfer reaction; (d) a transfer reaction that produces an excited fragment  $F'$  that equilibrates and subsequently decays by particle emission.

## EXPERIMENTAL RESULTS AT LOW BOMBARDING ENERGIES: THE TRANSITION REGION

There had been a number of measurements of heavy-ion spectra at bombarding energies less than  $\sim 10$  MeV/n that showed a quasi-elastic peak.<sup>11</sup> In these cases interest was focused on interpreting the most probable value of the distribution. The differences between the measured values and the beam velocity could be understood in large part with semiclassical models that assumed a two-body, or transfer, reaction.<sup>12</sup> One would expect that the momentum width in this case would be governed by the nuclear structure (i.e., strength functions and level densities) and kinematics of the system consisting of the target plus captured fragment. However, little attention was devoted to the widths of the quasi-elastic peaks.

Interest in the momentum widths increased dramatically when comparisons<sup>13</sup> of experimental data at 20 MeV/n were made with the results at relativistic energies. It seemed at first as if the transition from the smaller widths characteristic of low bombarding energies to the larger widths at high energies occurred at a remarkably low energy.<sup>2</sup> Experiments at smaller accelerators were pushed up in energy<sup>14-18</sup> and those at the high energy machines were pushed down in energy,<sup>19,20</sup> and new accelerators have been built<sup>21</sup> in order to explore this region. As a result we now know that the transition is accomplished within the region of 10–100 MeV/n. Figure 5 presents a summary of experimental reduced momentum widths,  $\sigma_0$ .

The reasons for the rapid increase in the momentum widths are not known. The understanding of this behavior is one of the outstanding problems in the study of heavy-ion reaction mechanisms. Attempts to understand these changes in  $\sigma$  naturally begin with an understanding of the asymptotic regions. Having examined the reaction mechanisms characteristic of the high-energy region, we now consider the low bombarding energies.

## THE LOWER ENERGIES: TRANSFER AND BREAK-UP

While it may be a safe assumption that a nucleon contained in a projectile moving with 2000 MeV/n will not be captured by the target nucleus and reach equilibrium, it is certainly not true at lower bombarding energies (< 20 MeV/n). Here, the projectile can transfer

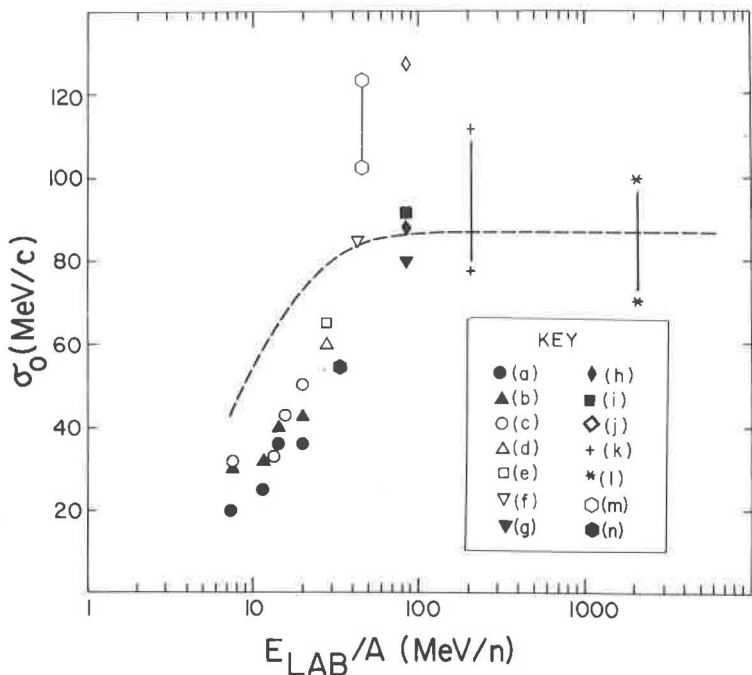


FIGURE 5 Reduced momentum widths  $\sigma_0$  obtained in a variety of reactions, as a function of projectile bombarding energy. Data points connected by a vertical line (44,213 and 2,100 MeV/n) indicate the range of widths obtained for a set of fragments from a given reaction. Although the rapid change in widths in the transition region is clear whether the actual widths  $\sigma$  or the reduced widths  $\sigma_0$  are considered, the data show less scatter when  $\sigma_0$  is plotted. The key is as follows: (a)  $^{197}\text{Au}$  ( $^{20}\text{Ne}, ^{16}\text{O}$ ), Ref. 14; (b)  $^{197}\text{Au}$  ( $^{20}\text{Ne}, ^{12}\text{C}$ ), Ref. 14; (c)  $^{208}\text{Pb}$  ( $^{16}\text{O}, ^{12}\text{C}$ ), Ref. 15; (d)  $^{197}\text{Au}$  ( $^9\text{Be}, ^7\text{Li}$ ), Ref. 17; (e)  $^{197}\text{Au}$  ( $^9\text{Be}, ^6\text{Li}$ ), Ref. 17; (f)  $^{181}\text{Ta}$  ( $^{20}\text{Ne}, \alpha$ ), Refs. 16, 18; (g)  $^{12}\text{C}$  ( $^{12}\text{C}, ^6\text{Li}$ ), Ref. 20; (h)  $^{12}\text{C}$  ( $^{12}\text{C}, ^7\text{Li}$ ), Ref. 20; (i)  $^{12}\text{C}$  ( $^{12}\text{C}, ^7\text{Be}$ ), Ref. 20; (j)  $^{12}\text{C}$  ( $^{12}\text{C}, ^{10}\text{B}$ ), Ref. 20; (k)  $^{232}\text{Th}$  ( $^{40}\text{Ar}, X$ ), Ref. 8; (l) Be — Pb ( $^{16}\text{O}, X$ ), Ref. 1; (m) Ni, Au ( $^{40}\text{Ar}, X$ ), Ref. 21; (n)  $^{181}\text{Ta}$  ( $^{10}\text{B}, \alpha$ ), Refs. 18, 19. See also Ref. 37. The dashed line is a calculation based on a peripheral model<sup>6</sup> appropriate for  $^{20}\text{Ne} + \text{Au}$ , normalized to  $\sigma_0 = 86$  MeV at high energies.

mass to the target and, at energies near the Coulomb barrier, this is a most likely outcome. Theoretical predictions of  $\sigma$  at low bombarding energies, therefore, must contend with two distinct processes depending on whether the missing mass was captured\* by the target.

\*By "captured" we mean that the transferred nucleon (or cluster of nucleons) was in a bound or continuum state of the target-plus-nucleon system during a time long enough for the rest of the projectile to leave the collision region.

In the case of capture, we refer to a transfer reaction, as in Figure 4c. Otherwise, we use the generic term, "break-up reaction," Figure 4a,b. (A separation of these two mechanisms is made possible by the use of a streamer chamber,<sup>22</sup> a device that visually records the tracks of the associated charged particles.) It is clear that combinations of these processes can occur, e.g., the projectile first picks up or loses mass, thus producing a fragment in a long-lived excited state that subsequently decays by particle emission (Figure 4d). Indeed, these two-step processes have been observed.<sup>23</sup>

McVoy and Nemes<sup>24</sup> have presented a calculation of the reaction  $^{208}\text{Pb}(^{16}\text{O}, ^{12}\text{C})$  for both these processes using a plane-wave approximation. The difference between transfer (Figure 4c) and fragmentation (Figure 4a) is contained in the wavefunction of the remaining nucleons  $R$  (in this case an alpha particle). In the case of fragmentation it is a plane wave with a distribution of momenta given by the Fermi momentum of the nucleons in the projectile. In the case of transfer, however, the wavefunction of the transferred nucleons is confined to the target. This confinement and conservation of momentum place additional constraints on the momentum of the observed fragment and result in a narrower distribution. Thus, it is possible that the increase in the widths shown in Figure 5 could arise from the predominance of transfer reactions at low energies and fragmentation reactions at high energies, and that the transition region reflects the competition between these processes, one having a narrow width and the other a broad width. Calculations made over a wide range of energy using the more elaborate distorted wave approximation<sup>25,26</sup> would be valuable.

The effect of the Coulomb barrier in the entrance channel is predicted to have a similar effect on the widths of *both* transfer and fragmentation processes.<sup>6,24</sup> It is the *local* momenta of the participants in the collision that affects the phase space available for the reaction. These momenta must be evaluated at the top of the Coulomb barrier  $V$  and are thus effectively reduced by the Coulomb potential. The dashed line in Figure 5 shows the variation in the width for the fragmentation of Ne by Au given by the factor  $(1 = V/E)^{1/2}$ , where  $E$  is the bombarding energy. The dashed line, arbitrarily normalized to 86 MeV/c at high energies, accounts for some of the energy dependence but does not reproduce the overall shape very well. It is of course possible that the momentum widths for both transfer and break-up processes have similar magnitudes and energy dependences

even though the relative strengths vary with energy. We simply do not know the answer yet.

## ADEQUACY OF THE EXISTING EXPERIMENTAL DATA

There are several difficulties encountered in analyzing the existing experimental data. Momentum is also imparted to the projectile fragments through their interaction with the target. A sideward deflection from repulsive Coulomb and attractive nuclear forces introduces a momentum dispersion,  $\sigma_{\perp}$ , perpendicular to the beam direction. The quantities  $\sigma_{\parallel}$  and  $\sigma_{\perp}$  may be deduced by measuring momentum distributions at different scattering angles, but often the experimental data consist of total momentum widths obtained from data at a single angle, and these are compared with theoretical predictions or scaling relations that are valid only for  $\sigma_{\parallel}$ . These considerations are important at the lower bombarding energies and have been discussed by Van Bibber *et al.*<sup>27</sup> and by Wong.<sup>28</sup>

Another problem concerns the deduction of a width from a spectrum that does not have a Gaussian shape (Figure 1). The results then may depend on the specific method or procedure chosen to fit the momentum spectrum. The application of uniform methods by different authors to determine the width of a distribution will be necessary to establish quantitatively the "fine structure" in the dependence of  $\sigma_0$  on mass and energy. These considerations,<sup>14,15</sup> while important when making precise comparisons either with theory or among experimental data, should not affect the overall energy dependence of  $\sigma_0$  as given in Figure 5 and it is this gross systematic behavior that is yet to be explained.

By far the most serious problem with the experimental data shown in Figure 5, however, is their inclusive nature. Only one particle has been observed in a given reaction and, therefore, all possible reaction mechanisms that can produce a single fragment with the characteristics of the observed particle may contribute. The most direct illustration of this problem is the situation at the lower bombarding energies in which both transfer reactions and break-up reactions are known to contribute to the inclusive yield.<sup>22</sup> It is through more elaborate, exclusive experiments that we can hope to make significant advancements in the understanding of peripheral heavy-ion reactions in general and momentum widths in particular.

## EXCLUSIVE MEASUREMENTS

A number of two-particle correlation experiments have been made at low bombarding energies and with sufficient precision to detect the presence of intermediate states or final-state interactions (Figure 4b,d). In nearly all cases in which two fragments were detected, the sum of which equaled the projectile, the reaction was shown to proceed via the two-step process



i.e., the relative kinetic energy of fragments *C* and *D* define a resonance or excited state in the projectile.<sup>23,29-31</sup> The lifetime for this state is sufficiently long that the excited projectile decays long after it has left the vicinity of the target nucleus. An example of this is shown in Figure 6. The relative kinetic energy of an  $\alpha$  particle and an  $^{16}\text{O}$  nucleus, produced in the break-up of  $^{20}\text{Ne}$ , has been deduced through a precise measurement of the positions and energies of the two particles.<sup>30</sup> Known excited states in  $^{20}\text{Ne}$  are indicated.<sup>30</sup> It appears now that break-up reactions proceed primarily through a two-stage process involving a direct reaction (inelastic scattering or transfer) that produces a fragment in an excited state that subsequently decays by particle emission. Prompt fragmentation (Figure 4a), which is usually assumed to occur and dominate at relativistic energies, has been observed in a heavy-ion reaction at low bombarding energies in only one special case (for  $^7\text{Li}$  projectiles).<sup>32</sup>

The two-particle exclusive measurements at low energies are generally made with silicon detectors having small solid angles and therefore it is difficult (though not impossible) to deduce the relative strengths of different processes. Detector systems having a  $4\pi$  solid angle make this much easier. Two such devices that have come into operation recently and have been used at nonrelativistic energies are the neutron ball at the Hahn-Meitner Institute<sup>33</sup> and the "Plastic Box" at the LBL 88-Inch Cyclotron.<sup>34</sup> The first device measures the total number of neutrons in coincidence with a given projectile fragment. For a heavy target, which decays primarily by neutron emission, the neutron multiplicity is a measure of the excitation energy acquired by the target, which in turn is an indicator of the mass transferred from the projectile to the target. The multiplicities associated with four or more missing mass units show two components

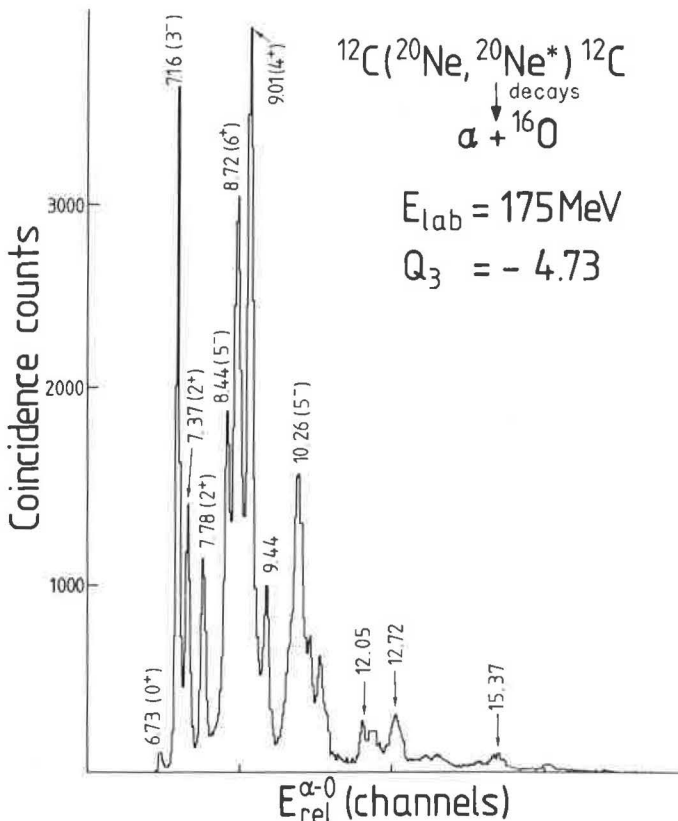


FIGURE 6 The relative kinetic energy of alpha particles and  $^{16}\text{O}$  ions, produced in the break-up of 8.7 MeV/n  $^{20}\text{Ne}$  ions.<sup>30</sup> The detected  $^{16}\text{O}$  and the unobserved  $^{12}\text{C}$  recoil are in their ground states. Precise measurement of the angles of the  $\alpha$ -particle and the oxygen ion ( $\pm \frac{1}{2}^\circ$ ) with position-sensitive silicon detectors is responsible for the high resolution. All the yield is accounted for by inelastic scattering to excited states of  $^{20}\text{Ne}$  (energies, spins, and parities are indicated) that subsequently alpha decay.

of comparable intensity. The high multiplicity component indicates a transfer reaction, the component at low multiplicity a break-up reaction. There are, of course, other ways of “tagging” the target-like fragment to determine if a transfer reaction took place. Observing characteristic x-radiation is an example.<sup>35</sup>

The plastic box, and its forerunner, the streamer chamber,<sup>22</sup> do not focus on the target-like fragment but rather detect the presence

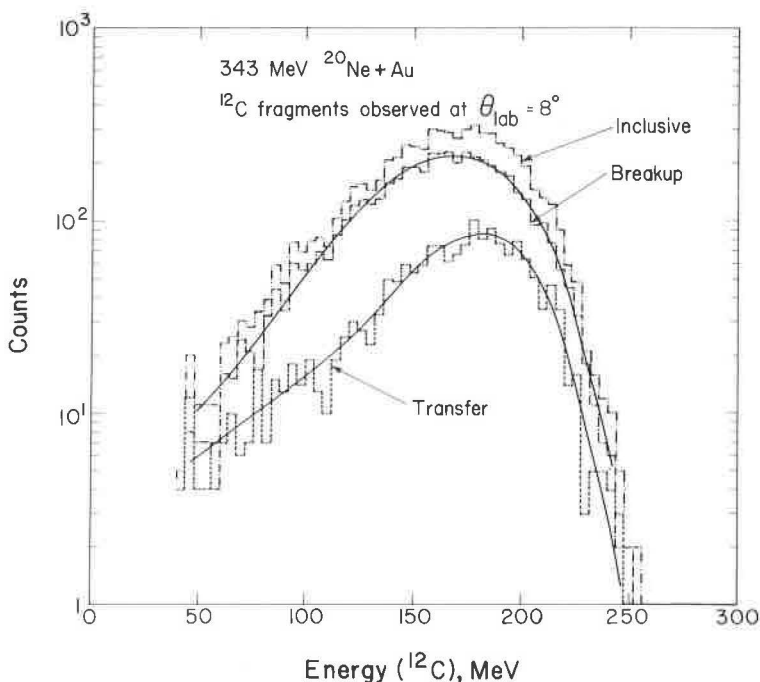


FIGURE 7 Spectra of projectile-like fragments at  $8^\circ$  in the reaction of 17.3 MeV/n Ne with Au.<sup>34</sup> The curve labeled transfer indicates fragments for which no charged particle was recorded by the  $4\pi$  detector. The events labeled break-up are all those having one or more charged particles (typically  $\alpha$ -particles or protons) in coincidence with the observed  $^{12}\text{C}$  nucleus.

or absence of charged particles associated with a given projectile fragment. If charged-particle decay by an excited target-like residual can be neglected, then the absence of any associated charged particles implies that the charge missing from the projectile after the collision was transferred to the target. Break-up reactions would have one or more charged particles in coincidence with the fragment observed in a counter telescope. Whereas the streamer chamber depends on visual observation of tracks in a photograph, the plastic box uses thin (1 mm) scintillator paddles to register charged particles. Energy spectra of  $^{12}\text{C}$  nuclei produced by the bombardment of gold by 17 MeV/n  $^{20}\text{Ne}$  ions are shown in Figure 7. The transfer component (no associated charged particles) is shifted toward higher energies and has a narrower width. One observes significant cross sections for the trans-

fer of up to seven charge units, i.e., a nitrogen nucleus. (The transfer of an  $^{16}\text{O}$  undoubtedly occurs as well, although this particular experiment was not sensitive to it.) From data such as these one can obtain the momentum widths separately for the transfer reactions. Early indications are that the behavior of the widths is complicated: there are some cases in which the transfer reaction has the broader width.

Exclusive measurements at relativistic energies naturally require instrumentation quite different in scope from the devices just described. The Heavy Ion Spectrometer System (HISS) at the Bevalac consists of a large (1-m diameter, 1-m gap) superconducting dipole and a variety of large detector systems that enable reconstruction of the trajectories of the charged projectile-like fragments emerging in the forward direction. Measuring the charge, mass, and momentum of each fragment permits the determination of the energy and momentum transferred to the projectile. [At low bombarding energies this can be done quite accurately, as evidenced by the high resolution ( $\sim 100$  keV) shown in Figure 6.] The goal for HISS is to obtain a resolution of  $\sim 2$  MeV for  $2.1 \text{ GeV/n } ^{12}\text{C}$  projectiles. This would make possible the identification of sequential processes (Figure 4b,d) provided they proceed at low excitation energies where the density of levels is of the order of the experimental resolution.

## SUMMARY

Nuclei that are clearly the remnants of the projectile are observed in all reactions in which the bombarding energy is from a few MeV per nucleon above the barrier up to 2000 MeV/n. The widths of the momentum distributions of the fragments change rapidly in the region of bombarding energy from 20 to 100 MeV/n. While it is possible to reproduce the gross behavior of the inclusive widths in the low or the high energy region with a variety of models, a satisfactory unified description that includes the transition region remains to be developed. The inclusive experimental results that have prompted the statistical model and its variations are inadequate to distinguish among the different models. At low and intermediate energies, two mechanisms, transfer and sequential decay, are known to contribute. Further study of the reaction mechanism requires exclusive measurements, a number of which are now being made, and many more

measurements in the intermediate energy region. This latter region, which for historical reasons is the last to be explored, is of particular interest and will receive increasing attention in the future. Basic questions, however, remain unanswered:

- (1) Does the reaction mechanism at relativistic energies really sample the Fermi momentum distribution prior to the collision, or are there significant components of thermalization and sequential decay that affect the observed values of  $\sigma$ ?
- (2) What is the bombarding energy dependence of  $\sigma$  for each of the separate mechanisms, transfer and break-up? At present this separation has been made for only one reaction at a few bombarding energies.
- (3) What is the origin of the rapid increase in  $\sigma_0$  and how do the different mechanisms sketched in Figure 4 contribute?

Additional questions undoubtedly will arise as further experiments in the transition region reveal variations in  $\sigma_0$  about the gross trend indicated in Figure 5. Already there are suggestions that there may be significant deviations from an otherwise smooth behavior. Even though it is 10 years since the first measurements with high energy heavy ions, the study of projectile fragmentation is still in its infancy.

#### Acknowledgment

This work was supported by the Director, Office of Energy Research, Division of Nuclear Physics of the Office of High Energy and Nuclear Physics of the U.S. Department of Energy under Contract DE-AC03-76SF00098.

R. G. STOKSTAD  
*Nuclear Science Division,  
Lawrence Berkeley Laboratory,  
University of California,  
Berkeley, California 94720*

#### References

1. D. E. Greiner, P. J. Lindstrom, H. H. Heckman, B. Cook, and F. S. Bieser, Phys. Rev. Lett. **35**, 152 (1975); D. L. Olson, B. L. Berman, D. E. Greiner, H. H. Heckman, P. J. Lindstrom, and H. J. Crawford, Phys. Rev. C **28**, 1602 (1983).
2. C. K. Gelbke, C. Olmer, M. Buenerd, D. L. Hendrie, J. Mahoney, M. C. Mermaz, and D. K. Scott, Phys. Rep. **42**, 311 (1978); C. K. Gelbke, in *Deep Inelastic and*

*Fusion Reactions with Heavy Ions*, edited by W. Von Oertzen, Lecture Notes in Physics Vol. 117 (Springer Verlag, New York, 1980) p. 210.

3. H. Feshbach and K. Huang, Phys. Lett. **47B**, 300 (1973); H. Feshbach and M. Zabek, Ann. Phys. (N.Y.) **107**, 110 (1977).
4. A. S. Goldhaber, Phys. Lett. **53B**, 306 (1974).
5. G. Bertsch, Phys. Rev. Lett. **46**, 47 (1981).
6. W. A. Friedman, Phys. Rev. C **27**, 569 (1983).
7. M. J. Murphy, Phys. Lett. **135B**, 25 (1984).
8. Y. P. Viyogi, T. J. M. Symons, P. Doll, D. E. Greiner, H. H. Heckman, D. L. Hendrie, P. J. Lindstrom, J. Mahoney, D. K. Scott, K. Van Bibber, G. D. Westfall, H. Wieman, H. J. Crawford, C. McParland, and C. K. Gelbke, Phys. Rev. Lett. **42**, 33 (1979).
9. V. K. Lukyonov and A. I. Titov, Phys. Lett. **57B**, 10 (1975).
10. J. Hüfner, K. Schäfer and B. Schürmann, Phys. Rev. C **12**, 1888 (1975).
11. R. N. Kaufmann and R. Wolfgang, Phys. Rev. **121**, 192 (1961); V. V. Volkov, G. F. Fridnev, G. N. Zorin, and L. P. Chelnokov, Nucl. Phys. A **126**, 1 (1969).
12. P. J. Siemens, J. P. Bondorf, D. H. E. Gross, and F. Dickman, Phys. Lett. **36B**, 24 (1971); B. G. Harvey and M. J. Murphy, Phys. Lett. **130B**, 373 (1983).
13. M. Buenerd, C. K. Gelbke, B. G. Harvey, D. L. Hendrie, J. Mahoney, A. Menchaca-Rocha, C. Olmer, and D. K. Scott, Phys. Rev. Lett. **37**, 1191 (1976); C. K. Gelbke, M. Buenerd, D. L. Hendrie, J. Mahoney, M. C. Mermaz, C. Olmer, and D. K. Scott, Phys. Lett. **65B**, 227 (1976); C. K. Gelbke, D. K. Scott, M. Bini, D. L. Hendrie, J. L. Laville, J. Mahoney, M. C. Mermaz, and C. Olmer, Phys. Lett. **70B**, 415 (1977).
14. Ch. Egelhaaf, G. Bohlen, H. Fuchs, A. Gamp, H. Homeyer, and H. Kluge, Phys. Rev. Lett. **46**, 83 (1981).
15. B. G. Harvey, Phys. Rev. Lett. (Comments) **47**, 454 (1981).
16. J. B. Natowitz, M. N. Namboodiri, L. Adler, R. P. Schmitt, R. L. Watson, S. Simon, M. Berlanger, and R. Choudhury, Phys. Rev. Lett. **47**, 1114 (1981).
17. M. Murphy and R. G. Stokstad, Phys. Rev. C **28**, 428 (1983).
18. J. B. Natowitz, Nucl. Phys. A **387**, 65C (1982).
19. M. N. Namboodiri, R. K. Choudhury, J. B. Natowitz, K. Hagel, L. Adler, P. L. Gonthier, H. Simon, S. Kniffen, R. Patton, E. Thomasi, C. Ngo, C. Mazur, and M. Ribrag, Phys. Rev. C **28**, 460 (1983).
20. J. Mougey, R. Ost, M. Buenerd, A. J. Cole, C. Guet, D. Lebrun, J. M. Loiseaux, P. Martin, M. Maurel, E. Monnand, H. Nifenecker, P. Perrin, J. Pinston, C. Ristori, P. de Saintignon, F. Schissler, L. Carlen, B. Jakobsson, A. Öskarsson, I. Otterluund, B. Schroder, H. A. Gustafsson, T. Johansson, H. Ryde, J. P. Bondorf, O. B. Nielsen, G. Tibell, Phys. Lett. **105B**, 25 (1981).
21. V. Borrel, D. Guerreau, J. Galin, B. Gatty, D. Jacquet, and X. Tarrago, Z. Phys. A **314**, 191 (1983).
22. M. J. Murphy, B. G. Harvey, D. L. Hendrie, W. W. Pang, K. Van Bibber, and R. Legrain, Phys. Lett. **120B**, 75 (1983).
23. R. K. Bhownik, J. Van Driel, R. H. Siemssen, G. J. Balster, P. B. Goldhoorn, S. Gonggrajp, Y. Iwasaki, R. V. F. Janssens, H. Sakai, K. Siwek-Wilczynska, W. A. Sterrenburg, and J. Wilczynski, Nucl. Phys. A **30**, 117 (1982).
24. K. W. McVoy and M. C. Nemes, Z. Phys. A **295**, 177 (1980).
25. T. Udagawa, T. Tamura, T. Shimoda, H. Fröhlich, M. Ishihara, and K. Nagatani, Phys. Rev. C **20**, 1949 (1979).
26. E. Takeda, T. Shimoda, N. Takahashi, T. Yamaya, K. Nagatani, T. Udagawa, and T. Tamura, Phys. Rev. C **22**, 772 (1981).
27. K. Van Bibber, D. L. Hendrie, D. K. Scott, H. H. Wieman, L. S. Schroeder, J.

- V. Geaga, S. A. Chessin, R. T. Treuhaft, Y. J. Grossiord, J. O. Rasmussen, and C. Y. Wong, Phys. Rev. Lett. **43**, 840 (1979).
28. C. Y. Wong and K. Van Bibber, Phys. Rev. C **25**, 2990 (1982).
29. J. Van Driel, S. Gonggrijp, R. V. F. Janssens, R. H. Siemssen, K. S. Wilczynska, and J. Wilczynski, Phys. Lett. **98B**, 351 (1981).
30. W. D. Rae, A. J. Cole, A. Dacal, R. Legrain, B. G. Harvey, J. Mahoney, M. J. Murphy, R. G. Stokstad, and I. Tserruya, Phys. Lett. **105B**, 417 (1981), and to be published.
31. H. Homeyer, M. Bürgel, M. Clover, Ch. Egelhaaf, H. Fuchs, A. Gamp, D. Kovar, and W. Rauch, Phys. Rev. C **26**, 1335 (1982).
32. A. C. Shotter, A. N. Bice, J. M. Wouters, W. D. Rae, and J. Cerny, Phys. Rev. Lett. **46**, 12 (1981).
33. A. Jahnke, G. Ingold, H. Homeyer, M. Burgel, Ch. Egelhaaf, H. Fuchs, and D. Hilscher, Phys. Rev. Lett. **50**, 1246 (1983).
34. K. Van Bibber, P. J. Countryman, M. J. Murphy, Y. D. Chan, R. G. Stokstad, I. Tserruya, and S. Wald, Lawrence Berkeley Laboratory Report No. LBL-16799; S. Wald, C. R. Albiston, M. Bantel, Y. D. Chan, B. G. Harvey, M. J. Murphy, I. Tserruya, R. G. Stokstad, P. J. Countryman, K. Van Bibber, and H. Homeyer, Lawrence Berkeley Laboratory Report No. LBL-16899.
35. H. W. Wilschut, R. K. Bhowmick, P. B. Goldhoorn, J. F. W. Jansen, R. H. Siemssen, K. Siwek-Wilczynska, Z. Srijkowski, and J. Wilczynski, Phys. Lett. **123B**, 173 (1983).
36. D. E. Greiner, Proc. Int'l. Conference on Nucleus Nucleus Collisions, Michigan State University, East Lansing, Michigan, 1982, Lawrence Berkeley Laboratory Report No. LBL-15071.
37. A. Menchaca-Rocha, M.E. Brandan, M. Buenerd, J. Chauvin, D. Lebrun, P. Martin, P. deSantignon, J. C. Gondrand, I. Dorion, and A. Lounis, Phys. Lett. **131B**, 31 (1983).